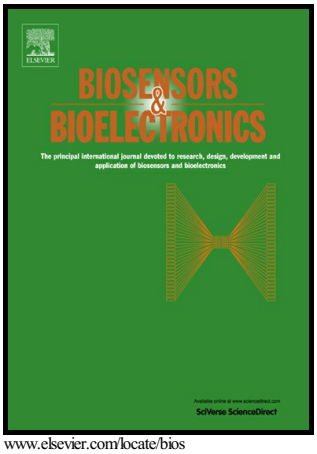

www.elsevier.com/locate/bios

Aldehyde functionalized ionic liquid on electrochemically reduced graphene oxide as a versatile platform for covalent immobilization of biomolecules and biosensing

Devaraj Manoj, K. Theyagarajan, Duraisamy Saravanakumar, Sellappan Senthilkumar, Kathavarayan Thenmozhi

PII: S0956-5663(17)30835-7
DOI: https://doi.org/10.1016/j.bios.2017.12.030
Reference: BIOS10175

To appear in: *Biosensors and Bioelectronic*

Received date: 16 August 2017
Revised date: 18 December 2017
Accepted date: 20 December 2017

Cite this article as: Devaraj Manoj, K. Theyagarajan, Duraisamy Saravanakumar, Sellappan Senthilkumar and Kathavarayan Thenmozhi, Aldehyde functionalized ionic liquid on electrochemically reduced graphene oxide as a versatile platform for covalent immobilization of biomolecules and biosensing, *Biosensors and Bioelectronic,* https://doi.org/10.1016/j.bios.2017.12.030

Aldehyde functionalized ionic liquid on electrochemically reduced graphene oxide as a versatile platform for covalent immobilization of biomolecules and biosensing

Devaraj Manoj[1], K. Theyagarajan[1], Duraisamy Saravanakumar, Sellappan Senthilkumar* and Kathavarayan Thenmozhi*

Department of Chemistry, School of Advanced Sciences, VIT University, Vellore-632014, India.

*Corresponding Author: Tel: +914162202404; Email: senthilanalytical@gmail.com (Sellappan Senthilkumar), kt.thenmozhi@gmail.com (Kathavarayan Thenmozhi).

[1] Authors contributed equally to this work.

Abstract

An aldehyde functionalized ionic liquid, (3-(3-formyl-4-hydroxybenzyl)-3-methylimidazolium hexafluorophosphate) (CHO-IL) has been employed herein as a multiple host platform for the covalent immobilization of mediator as well as enzyme. The CHO-IL was immobilized on electrochemically reduced graphene oxide (ERGO) through the π-π stacking of hydroxybenzyl and imidazolium groups with ERGO and subjected to further covalent attachment of Azure A (Azu-A) mediator or glucose oxidase (GOx) enzyme. Electroactive, water soluble organic dye Azu-A was effectively immobilized to the host IL through simple Schiff base reaction. Azu-A was rendered leak-free in the electrode setup and also responded well for the amperometric determination of H_2O_2 over a linear range of 0.03 to 1 mM with a detection limit and sensitivity of 11.5 µM and 133.2 µA mM^{-1} cm^{-2}, respectively. Further, attempts were made to explore the CHO-IL platform for the covalent immobilization of GOx enzyme which served well in retaining the enzyme nativity, reactivity and stability. Under optimized conditions, mediatorless GOx biosensor developed based on direct electrochemistry has exhibited an impressive analytical signal towards glucose detection in the linear range of 0.05 to 2.4 mM with a detection limit and sensitivity of 17 µM and 17.7 µA mM^{-1} cm^{-2}, respectively. The reliability of the proposed Azu-A based chemical sensor and GOx based biosensor towards the determination of H_2O_2 and glucose in the real samples have been demonstrated. The remarkable analytical parameters and long term stability of both the sensors could be envisioned as a result of facile immobilization platform and immobilization strategy.

Keywords: azure A, glucose oxidase, ionic liquid, graphene oxide, electrocatalytic activity, Schiff base.

1. Introduction

A well-designed methodology and suitable matrix for immobilization of biomolecules and stabilization can become a powerful tool owing to its applications in distinct areas of fuel cells, catalysis and biosensing (Cao et al., 2013; Walcarius et al., 2013; Sassolas et al., 2012; Yang et al., 2018). Especially, researchers involved in the development of enzymatic biosensors give much emphasis in identifying appropriate matrices for enzyme immobilization in order to improve the properties of enzymes such as activity, specificity, selectivity and stability (Kim et al., 2017; Mondal et al., 2017). A large number of biosensors based on different immobilization protocols, constructed with variety of matrices based on organic supports (Erramuspe et al., 2016; Pauliukaite et al., 2010) and inorganic materials (Kumar-Krishnan et al., 2016; Etienne et al., 2015) have been reported, which have incrementally added advantage to the existing biosensors. Still the search and scope for new materials with well-defined properties for immobilization and detection of biomolecules is a compelling need for industrial and biotechnological applications (Zhang et al., 2017; Hui et al., 2016; Guohua et al., 2017; Jiaojiao et al., 2015).

Ionic liquids have gained potential application as environmentally benign media owing to the deck of properties including lower melting points, wide range of solubility, negligible vapour pressure, tunable miscibility and viscosity (Huddleston et al., 2001; Hagiwara et al., 2000). These ILs comprising organic cations and inorganic anions offers plethora of combinations that can be tuned to achieve desired physicochemical properties for specific application (Torimoto et al., 2010; Giernoth 2010). This tunability of ILs has rendered remarkable characteristics such as high ionic conductivity, non-flammability, biocompatibility and good electrochemical and thermal stability, which are desired for electrochemical applications (Armand et al., 2009; Hapiot

et al., 2008; Quinn et al., 2002). Accordingly, ILs have attracted worldwide recognition and opened the avenues for their application in biosensor (Kwak et al., 2014; Benjamin et al., 2017), biomedical (Pereiro et al., 2013), biocatalysis (Sprenger et al., 2017) and bioelectronics (Wasilewski et al., 2017). Integrating and exploiting the synthetic flexibility, tunability and biocompatibility of ILs for the immobilization of innumerable chemical entities and biomolecules is of great interest in the development of biosensors.

Enormous efforts have been dedicated towards development of electrochemical sensors and biosensors using carbon ionic liquid electrodes (CILEs) and reasonable progress has been achieved (Safavi et al., 2009; Huang et al., 2011; Sun et al., 2014; Chen et al., 2015; Haghighi et al., 2014). However, biosensors fabricated through the adsorption, entrapment, encapsulation, or chelation of enzyme or proteins by simple physical interaction always encounter the problem of leachability, leading to poor sensitivity or lack prolonged performance. Among different protocols, covalent immobilization of the biomolecules is an exciting goal as it offers rigidification and operational stabilization surpassing the limitations of other techniques (Zhang et al., 2010; Bai et al., 2014). Covalent immobilization of enzymes and proteins are achieved through the reactive functional groups on the substrate and the biomolecules using different coupling chemistry. Commonly employed immobilization strategies include glutaraldehyde crosslinking (Thenmozhi et al., 2017), carbodiimide crosslinking (Mahmoud et al., 2009; Ghica et al., 2009), biotinylation (Ballesta-Claver et al., 2012), etc. All these reactions demand inclusion of a crosslinker or tedious fabrication procedure. Hence, a facile route for enzyme immobilization devoid of all these cumbersome processes is always desirable.

The potential for molecular architecture of ILs with suitable functionalities could serve as the right host for anchoring mediators and biomolecules which are crucial in the development of

sensors and biosensors (Kwak et al., 2014; Maroneze et al., 2016). This motivated us in design and synthesis of an aldehyde functionalized IL, (3-(3-formyl-4-hydroxybenzyl)-3-methylimidazolium hexafluorophosphate) (CHO-IL). The CHO-IL was immobilized on electrochemically reduced graphene oxide (ERGO) deposited over screen printed carbon electrode (SPE). ERGO possesses high conductivity, large surface area and high defect density on edge-plane sites which allows fast electron transfer at the electrode surface and thus would facilitate the electrochemical sensing (Unnikrishnan et al., 2013). The free aldehydic functionality of IL could aid in direct immobilization of enzymes through a simple Schiff base reaction by the formation of an imine linkage between the enzyme and host IL. In addition, the benzyl and imidazolium groups of CHO-IL would bind strongly with ERGO through π-π stacking (Han et al., 2016) and the phenolic –OH group would enhance the sorption affinity of ERGO for CHO-IL (Yu et al., 2017). Azu-A, an organic dye is one of the derivatives of phenothiazine which exhibits excellent redox behaviour and is highly attractive in electrochemical sensing because of its lesser formal potential (Priya et al., 2012). Initially, Azu-A, containing free amino group has been chosen as a model compound to examine the potential of anchoring -NH_2 group over the –CHO group of host IL. This highly water soluble mediator has been rendered leak-free stability and exhibited prominent electrochemical behaviour in the new electrode setup attributable to the stable imine linkage. The new electrode system demonstrated a good sensitivity towards H_2O_2 and thus it was developed as a chemical sensor to detect H_2O_2.

After successfully establishing a chemical sensor with the proposed coupling chemistry, we further extended the immobilization strategy for the development of a mediatorless biosensor. On this aspect, GOx enzyme was linked to the aldehydic moiety of IL through Schiff base

reaction, which resulted in stable anchoring of the enzyme. Further, the developed biosensor exhibited good sensitivity towards glucose over a wide range. The prepared functional IL demonstrated to be an excellent anchoring site suiting both the mediator and the enzyme immobilization if otherwise would lead to signal loss due to dissolution of water soluble mediator Azu-A and highly soluble and sensitive GOx enzyme. Azu-A based chemical sensor and GOx based biosensor have exhibited impressive electrochemical performance towards the determination of H_2O_2 and glucose, respectively, paving way for clinical applications.

2. Experimental Section

All chemicals, materials and instrumentation details, spectral characterization of synthesized ionic liquids are detailed in supporting information (SI).

2.1. Synthesis of aldehyde functionalized IL (CHO-IL)

The aldehyde functionalized IL was synthesized through the following steps and the corresponding scheme is given as Figure 1.

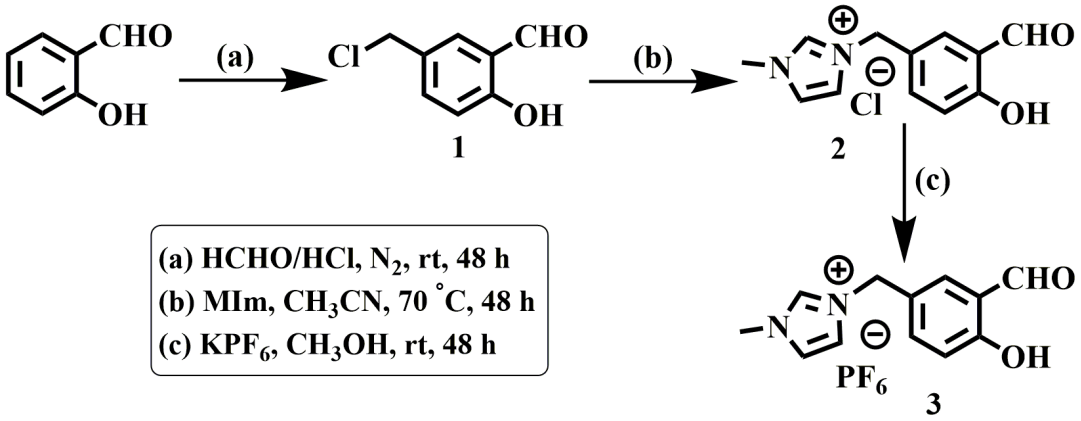

Figure 1. Synthesis procedure of aldehyde functionalized IL.

2.1.1 Synthesis of 5-chloromethyl-2-hydroxybenzaldehyde (1)

5-chloromethyl-2-hydroxybenzaldehyde was synthesized using the procedure reported earlier with slight modification (Benjamin et al., 2017). To a stirring mixture of hydrochloric acid (120 mL) and formaldehyde (24 mL), 19.2 g of salicylaldehyde (157.37 mmol) was added dropwise followed by the addition of 0.2 mL of sulphuric acid and stirring was continued for another 48 h under N_2 atmosphere. The resulting precipitate was separated out by filtration, washed several times with H_2O and finally dried under vacuum. Recrystallization from hot n-hexane gave the product (1) in 55.2 % (14.80 g) yield.

2.1.2 Synthesis of 3-(3-formyl-4-hydroxybenzyl)-3-methylimidazolium chloride (2)

1-methylimidazole (1.28 g, 15.59 mmol) dissolved in acetonitrile (20 mL) was added dropwise to the stirring solution of 5-chloromethyl-2-hydroxybenzaldehyde (1) (2.58 g, 15.12 mmol) in acetonitrile (35 mL) and the reaction mixture was refluxed at 70 ºC for 48 h. After cooling the reaction mixture to room temperature, the precipitate was collected by filtration, washed with diethyl ether (3 × 30 mL) and finally dried under vacuum to obtain a pale yellow solid (2) with 88 % (3.36 g) yield.

2.1.3. Synthesis of 3-(3-formyl-4-hydroxybenzyl)-3-methylimidazolium hexafluorophosphate (CHO-IL) (3)

The quaternized imidazolium chloride salt (2) (1.27 g, 5.02 mmol) was then readily metathesized with a methanolic solution of potassium hexafluorophosphate (0.936 g, 5.08 mmol) and the mixture was continuously stirred at room temperature for 48 h. After completion of the metathesis, the solvent was removed by rotary evaporation, and the residue was washed with ethyl acetate (3 × 30 mL). The product was dried at 60 ºC under vacuum for 6 h, to provide (3) as milky white solid in 85 % (1.54 g) yield.

2.2 Fabrication of Azu-A modified SPE

Graphene oxide (GO) was prepared using Hummers and Offeman's method (Hummers et al., 1958) after minor modification and the typical procedure along with the TEM image of GO are presented in the SI (Figure S1A). A bare SPE was electrochemically pre-anodized by applying a potential of 2.0 V for 300 s in 0.1 M phosphate buffer (pH 7.0) under constant stirring and dried under the stream of nitrogen. 5 µL of GO dispersion (0.1 mg/mL) was drop-cast over the pre-anodized SPE and allowed to dry in air to provide GO deposited SPE (GO/SPE). Then, GO was electrochemically reduced by subjecting the GO/SPE to potential cycling between 0 and -1.5 V in 0.1 M phosphate buffer (pH 7.0) at a scan rate of 50 mV s^{-1} until a constant current was achieved (Figure S1B). 10 µL of CHO-IL (2 mg/100 µL methanol) was drop-cast on the surface of the electrochemically reduced GO deposited SPE (ERGO/SPE), and allowed to dry to obtain aldehyde functionalized IL-immobilized ERGO/SPE platform (CHO-IL/ERGO/SPE). CHO-IL/ERGO/SPE was dipped into Azu-A solution (4 mg/mL phosphate buffer) for 2 h. Herein, Azu-A was covalently attached to the electrode surface through Schiff base condensation between aldehyde group of CHO-IL and amine group of Azu-A. The loosely adsorbed dye molecules were removed by washing the electrode with phosphate buffer to furnish Azu-A immobilized CHO-IL/ERGO/SPE (Azu-A/CHO-IL/ERGO/SPE). For comparison, Azu-A/CHO-IL modified SPE (Azu-A/CHO-IL/SPE) was also prepared in the absence of ERGO by adopting similar procedure to investigate the role of ERGO in the sensing performance.

2.3 Fabrication of GOx modified SPE

Glucose oxidase immobilized CHO-IL/ERGO/SPE (GOx/CHO-IL/ERGO/SPE) was developed by covalently immobilizing the enzyme GOx with CHO-IL on electrode surface, using the same procedure adopted for Azu-A/CHO-IL/ERGO/SPE, in place of Azu-A. The

CHO-IL/ERGO/SPE was dipped into a freshly prepared GOx solution in 0.1 M phosphate buffer (2 mg/mL) for 2 h. After the covalent immobilization of GOx, the electrode was carefully washed with copious amount of phosphate buffer, to remove the loosely bound enzyme moieties and the resulting GOx/CHO-IL/ERGO/SPE modified electrode was stored at 4 °C when not in use. Simultaneously, GOx/CHO-IL/SPE (without ERGO) has also been developed for comparison.

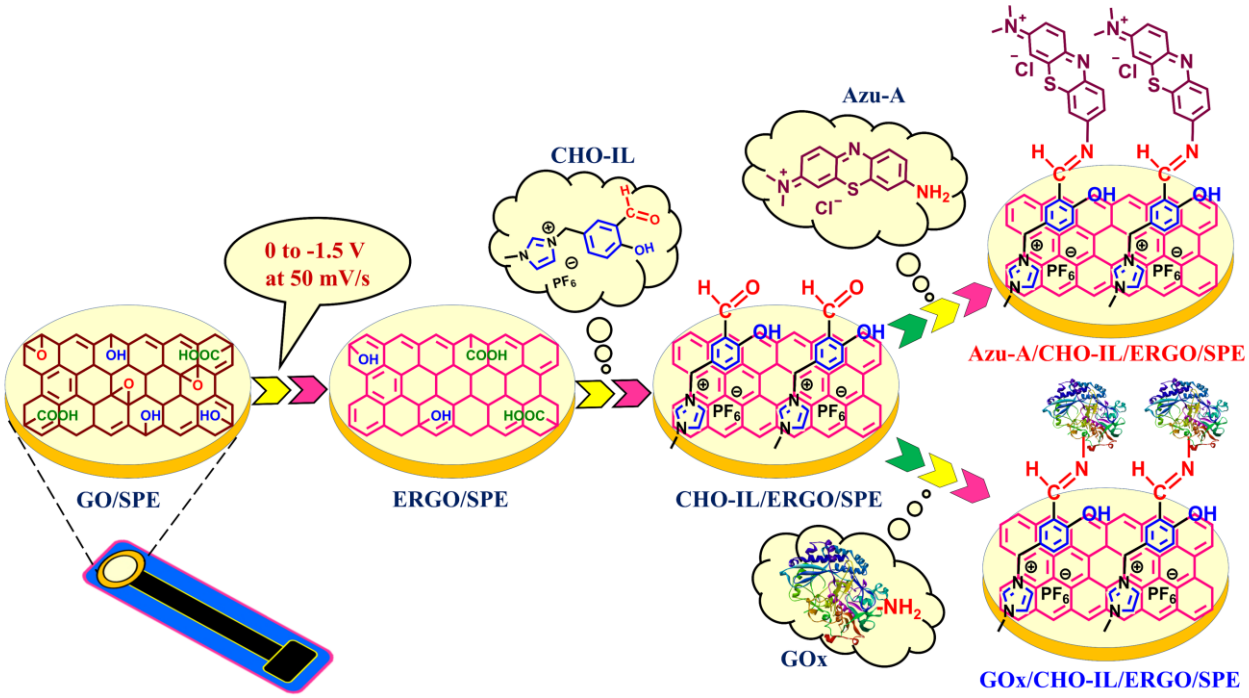

Figure 2. Schematic illustration of the steps involved in covalent immobilization of Azu-A and GOx on CHO-IL/ERGO/SPE platform.

3. Results and Discussion

The synthesized aldehyde functionalized ionic liquid was characterized using ^{1}H & ^{13}C NMR, FT-IR and HRMS spectra (Figure S6-S10). The CHO-IL immobilized on ERGO was

utilized as a platform for the covalent immobilization of Azu-A and GOx. The aldehydic functionality on the support IL and the free amino groups on the mediator/enzyme were taken advantage for specific interaction in covalent immobilization procedure. The stepwise electrode modification strategy has been illustrated in Figure 2.

3.1. Covalent immobilization of Azu-A and GOx on CHO-IL

The FTIR spectral analysis could provide a clear insight into the covalent binding of amino functionalities of Azu-A or GOx with the aldehyde group of CHO-IL through a Schiff base condensation. In this study, the samples were scratched off the modified electrode surfaces using a home-made needle which were allowed to dry under vacuum and then the spectra were recorded (Figure 3). FTIR spectrum of CHO-IL (black line) in Figure 3A and 3B displayed a sharp band at 1732 cm^{-1} which is the characteristic stretching vibration of aldehydic carbonyl group (-C=O) (Mandegani et al., 2016). The peaks observed at 1604 and 834 cm^{-1} correspond to the C=N (imidazole) and P-F groups of CHO-IL, respectively (Benjamin et al., 2017). The FTIR spectrum of Azu-A (green line) showed a band at 1602 cm^{-1} due to the –N-H bending vibration of free $–NH_2$ group (Snehalatha et al., 2009). In the case of Azu-A/CHO-IL (red line), the band at 1732 cm^{-1} of CHO-IL and 1602 cm^{-1} of Azu-A were found to disappear and a new intense peak at 1665 cm^{-1} was observed, indicating the imine bond (-C=N) formation through the condensation of -CHO and $-NH_2$ groups of CHO-IL and Azu-A, respectively (Mandegani et al., 2016). These results clearly indicate that Azu-A has been successfully immobilized onto CHO-IL via Schiff base reaction.

It is interesting to note that the GOx/CHO-IL (Figure 3B, blue line) exhibited a similar imine bond formation as that of Azu-A/CHO-IL. In the FTIR spectrum of GOx/CHO-IL, the carbonyl group (1732 cm^{-1}) of CHO-IL disappeared and a new peak emerged at 1659 cm^{-1} due to

the formation of an imine linkage with GOx molecules, evidencing the covalent functionalization between GOx and CHO-IL. The native GOx (magenta line) displays two distinct peaks at 1647 and 1554 cm^{-1} corresponding to amide I and amide II bands of GOx, respectively. It is well known that the disappearance of amide II absorption band specifies the typical behaviour of unfolding and denaturation of the enzyme at the modified electrode surface, mainly attributable to the immobilization strategy (Zhao et al., 2015; Liu et al., 2016). As per our aspiration, both the amide I and amide II bands were retained with a negligible shift in the FTIR spectrum of GOx/CHO-IL. This observation reveals that the GOx molecules are preserved in their native state, even after covalent immobilization with CHO-IL. The results further conclude that CHO-IL provide good biocompatibility and greater affinity for GOx in the electrode modification process.

3.2. Electrochemical impedance spectroscopy

The electrochemical impedance spectra (EIS) recorded in 0.1 M KCl containing 2.5 mM $[Fe(CN)_6]^{3-/4-}$, during every stage of modification are presented as Nyquist plot in Figure 3C. A Randles circuit was used to fit the impedance results (inset to Figure 3C) and the diameter on the semicircle is a direct representation of the charge transfer resistance (R_{ct}). The Nyquist plot of bare SPE exhibited a high R_{ct} of 350 Ω indicative of an insufficient electron transfer process at the surface of bare SPE. Upon the deposition of ERGO on SPE (ERGO/SPE), the R_{ct} significantly decreased to 246 Ω witnessing the increase in conductivity offered by ERGO. With CHO-IL/ERGO/SPE, a still smaller R_{ct} of 124 Ω was observed indicative of the low barrier on electron transfer contributed by the synergistic effect of ERGO and IL. On further modification with Azu-A, Azu-A/CHO-IL/ERGO/SPE showed a very low R_{ct} of 78 Ω, revealing the greater electron shuttling ability of the mediator. However, with GOx/CHO-IL/ERGO/SPE the

impedance increased significantly to R_{ct} of 474 Ω suggesting the hindrance for electron transfer through the dense protein layer of the non-conducting enzyme. On judging the EIS results, the new platform comprising ERGO and IL synergistically provides good conductivity and thus making them suitable for both electrochemical sensing and biosensing.

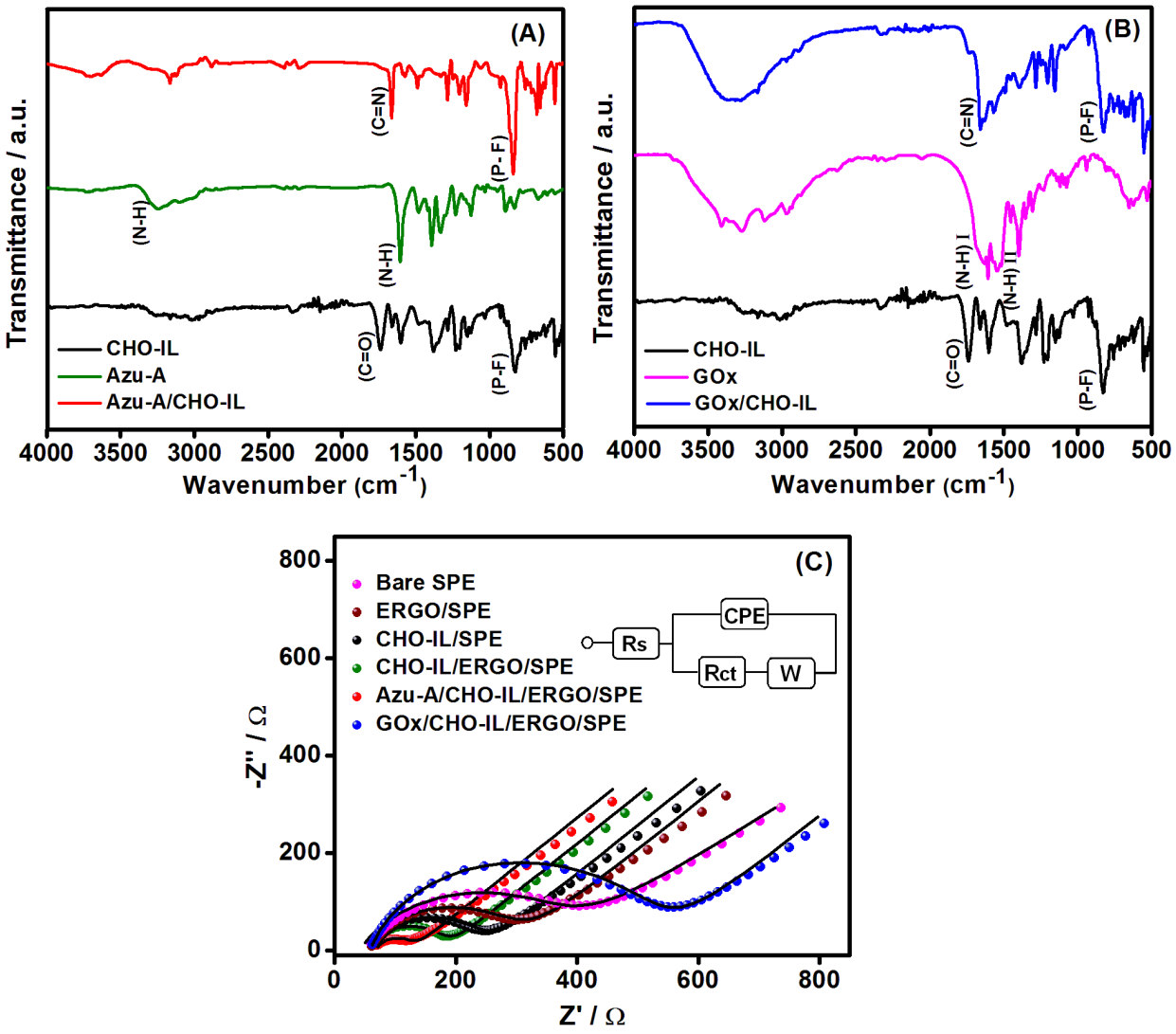

Figure 3. FT-IR spectra (A and B) of CHO-IL, Azu-A, Azu-A/CHO-IL, GOx and GOx/CHO-IL obtained at different modification stages during fabrication. (C) Nyquist plot obtained for bare SPE, ERGO/SPE, CHO-IL/SPE, CHO-IL/ERGO/SPE, Azu-A/CHO-IL/ERGO/SPE, GOx/CHO-

IL/ERGO/SPE in 0.1 M KCl containing 2.5 mM $[Fe(CN)_6]^{3-/4-}$ with proposed equivalent circuit as inset.

3.3. Electrochemical behavior and electrocatalytic activity of Azu-A/CHO-IL/ERGO/SPE

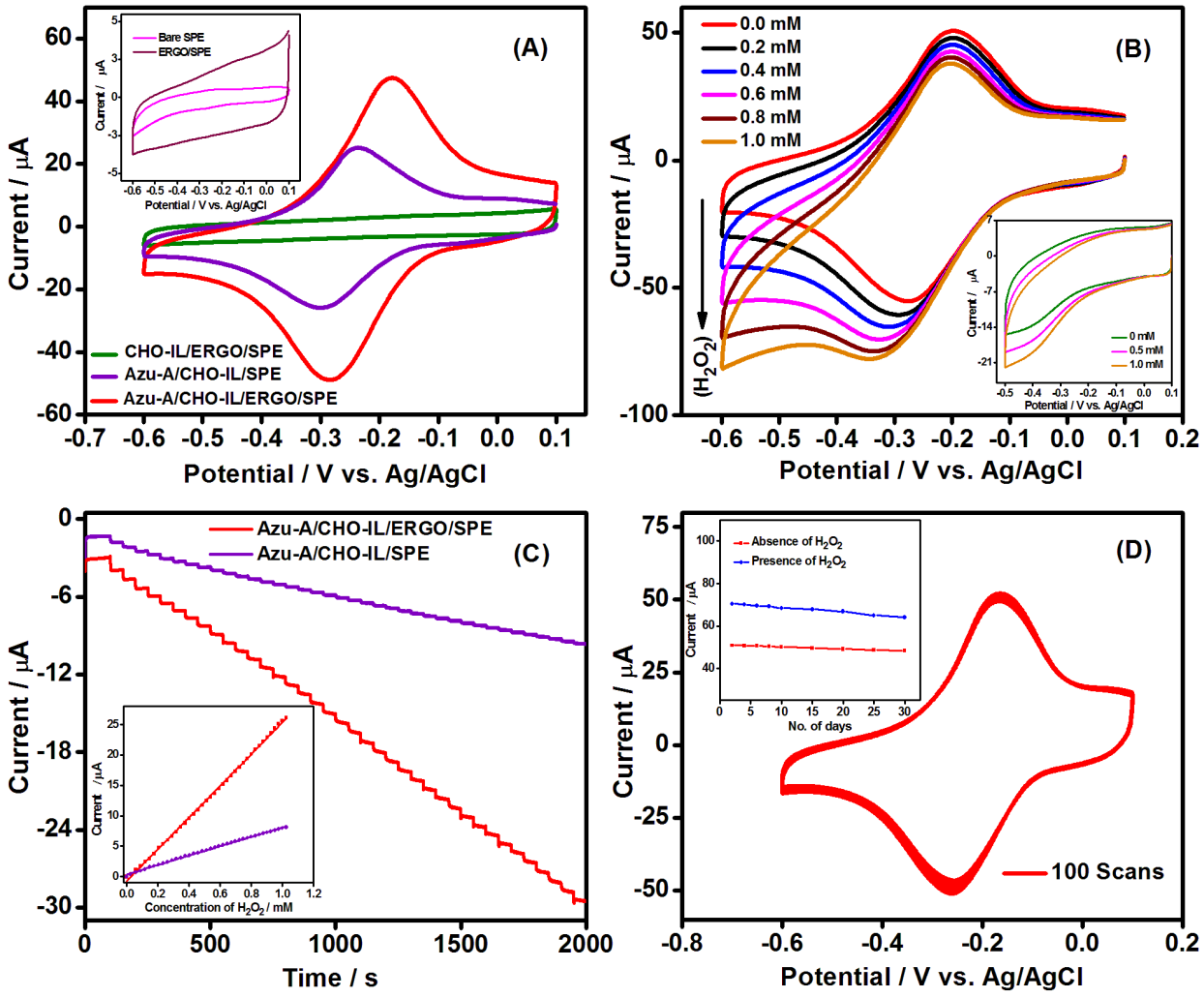

Figure 4. (A) CV curves of CHO-IL/ERGO/SPE, Azu-A/CHO-IL/SPE and Azu-A/CHO-IL/ERGO/SPE. Inset: CVs of bare and ERGO/SPE recorded under similar conditions. (B) CVs of Azu-A/CHO-IL/ERGO/SPE with increasing concentration of H_2O_2. Inset: CV curves of CHO-

IL/ERGO/SPE in presence of H_2O_2. (C) Amperometric response for Azu-A/CHO-IL/SPE and Azu-A/CHO-IL/ERGO/SPE on successive additions of 30 µM H_2O_2 into stirred electrolyte; Applied potential: -0.4 V. Inset: Calibration plots corresponding to the amperometric response. (D) CVs of Azu-A/CHO-IL/ERGO/SPE for 100 continuous cycles. Inset: Plot of day-to-day current response of the modified electrode in the absence and presence of 0.6 mM H_2O_2. Electrolyte: 0.1 M phosphate buffer (pH 7.0). Scan rate: 50 mV s^{-1}.

The voltammetric response of Azu-A immobilized on the newly developed CHO-IL/ERGO platform was investigated using cyclic voltammetry (CV). The electrochemical behaviour of the modified electrode was sequentially characterized during the modification process by recording the CV in N_2 saturated 0.1 M phosphate buffer (pH 7.0) at a scan rate of 50 mV s^{-1} and shown in Figure 4A. As anticipated, bare SPE, ERGO/SPE and CHO-IL/ERGO/SPE did not exhibit any redox peak indicating that SPE, ERGO and CHO-IL are not redox active in the potential window studied in the range of 0.1 to -0.6 V. The CV of Azu-A/CHO-IL/SPE exhibited a set of well-defined peaks owing to the redox behaviour of Azu-A, with anodic (E_{pa}) and cathodic (E_{pc}) peak potentials of -0.237 and -0.305 V, respectively and the formal potential ($E°$) was calculated to be -0.271 V. The voltammogram of Azu-A/CHO-IL/ERGO/SPE has also depicted similar redox peaks with E_{pa} and E_{pc} of -0.177 and -0.282 V with $E°$ of -0.230 V. A substantial increase in cathodic and anodic peak currents of the redox couple was observed for Azu-A/CHO-IL/ERGO/SPE, which is ascribed to the enhanced surface of ERGO along with its excellent conductivity. The immobilization of CHO-IL on ERGO through π-π stacking, followed by the covalent attachment of Azu-A sustained its well-resolved electrochemical behaviour.

The catalytic activity of Azu-A/CHO-IL/ERGO/SPE modified electrode was tested towards the electrochemical reduction of H_2O_2 (Figure 4B). Azu-A/CHO-IL/ERGO/SPE modified electrode displayed a typical electrocatalytic process, as observed with an increment in cathodic peak current for every addition of H_2O_2 at a potential of -0.35 V. Under similar conditions, the CHO-IL/ERGO/SPE responded to H_2O_2 feebly at a relatively higher onset reduction potential of -0.45 V (inset to Figure 4B). During the mediated electrocatalytic process, the Azu-A mediator gets reduced when its reduction potential is reached during the potential scan (eqn. 1). The reduced form of Azu-A in turn reduces the analyte H_2O_2 at the electrode-solution interface and consequently the mediator gets oxidized. The electrochemically reduced mediator is catalytically active for the chemical reduction of H_2O_2 (eqn. 2) and the reactions in eqns. 1 and 2 occur in a cyclic manner, resulting in the enhancement of cathodic current for every addition of H_2O_2. The enhanced electrocatalytic activity of Azu-A/CHO-IL/ERGO/SPE is accredited to the highly conducting IL and the enlarged electroactive surface area of ERGO which facilitates the Azu-A mediated reduction of H_2O_2.

$$\text{Azure A}_{(Oxd)} + 2e^- + 2H^+ \longleftrightarrow \text{Azure A}_{(Red)} \quad (1)$$

$$\text{Azure A}_{(Red)} + H_2O_2 \longrightarrow \text{Azure A}_{(Oxd)} + H_2O \quad (2)$$

Amperometric detection of H_2O_2 was performed at the modified electrode in order to authenticate the catalytic activity under dynamic conditions. As observed in Figure 4B, maximum catalytic current for H_2O_2 reduction was observed around -0.35 V and hence a slightly higher potential of -0.40 V was chosen as the optimum potential for amperometric sensing. Figure 4C displays the stable step wise amperometric response of Azu-A/CHO-IL/SPE and Azu-A/CHO-IL/ERGO/SPE for successive addition of H_2O_2 aliquots into a stirred supporting electrolyte solution of 0.1 M phosphate buffer (pH 7.0) at a constant potential of -0.40 V. The

response current enhanced rapidly and reached a steady state value within 3 s at both the modified electrodes, revealing the fast electron transfer efficiency of Azu-A in the immobilized electrode setup and the effective electrochemical reduction of H_2O_2 at the electrode surface. Inset to Figure 4C compares the calibration curves constructed for the determination of H_2O_2 at Azu-A/CHO-IL/SPE and Azu-A/CHO-IL/ERGO/SPE. The current response recorded at Azu-A/CHO-IL/ERGO/SPE was proportional to H_2O_2 concentration in the linear range of 0.03 to 1 mM, beyond which the calibration curve deflexed gradually. The sensitivity and detection limit was estimated to be 133.2 µA mM^{-1} cm^{-2} and 11.5 µM at a signal to noise ratio of 3 respectively. It can be observed that Azu-A/CHO-IL/ERGO/SPE exhibited a relatively higher sensitivity than Azu-A/CHO-IL/SPE (39.6 µA mM^{-1} cm^{-2}) owing to the additional conductivity offered by ERGO. The performance of Azu-A/CHO-IL/ERGO/SPE in terms of wide linear range and low detection limit are comparable or better than the recently reported non-enzymatic sensors for H_2O_2 (Table S1). The observed results are devoted to the fast electron shuttling ability of the Azu-A benefited through the high conductivity furnished by both ERGO and the covalently tethered IL in the modified electrode.

The operational stability, long-term performance and reproducibility also play a critical role in deciding the efficacy of the developed sensor. Azu-A/CHO-IL/ERGO/SPE was subjected to 100 potential cycles in the range of 0.1 V to -0.6 V at 50 mV s^{-1}, which revealed that the sensor was significantly stable with no obvious alteration in cathodic and anodic peak currents and potentials (Figure 4D). The long-term working of the model sensor was examined in the absence and presence of 0.6 mM H_2O_2 over a period of 30 days. Inset to Figure 4D illustrates that the sensor retained 95 % of the response in the absence of H_2O_2 and recovered 91 % response towards 0.6 mM H_2O_2. During the fabrication of 5 individual electrodes, a good

reproducibility of the response current was achieved for sensing 0.6 mM H_2O_2, with a relative standard deviation of 1.81 % (Figure S12). The results indicate that the proposed sensor demonstrated credible stability, long-term operational consistency and reproducibility owing to the firm covalent anchoring of the highly water soluble Azu-A.

The selectivity of the sensor was assessed by adding 0.5 mM of electroactive species such as KIO_3, $KBrO_3$, $NaNO_2$, L-cysteine, glucose, ascorbic acid, dopamine, uric acid and citric acid along with 50 µM concentration of H_2O_2 and the detection was carried out using amperometry at a potential of -0.40 V. As seen in Figure S13, even 10 times higher concentration of these species did not alter the response current appreciably, wherein only H_2O_2 injection gave remarkable current response. The observed results indicate that the Azu-A/CHO-IL/ERGO/SPE exhibits reasonable selectivity towards the determination of H_2O_2.

The practical applicability of the Azu-A/CHO-IL/ERGO/SPE was checked by the detection of H_2O_2 in milk samples, as often H_2O_2 is an additive introduced for preservation of food products. Known concentrations of H_2O_2 were spiked into the milk and apple juice samples by standard addition method and monitored their recovery at a working potential of -0.40 V using amperometry. Figure S14 shows that every spike of H_2O_2 aliquot has responded with steep and steady reduction current at the modified electrode. The results (Table S2) reveal that the recoveries were in the range of 97.3 to 103.3 % suggesting that the proposed H_2O_2 sensor has a great potential in real sample analysis.

3.4. Direct electrochemistry of GOx at GOx/CHO-IL/ERGO/SPE

The aldehyde functionalized IL has demonstrated to be a suitable host matrix for the immobilization of the model system Azu-A. The successful demonstration of H_2O_2 sensing by Azu-A/CHO-IL/ERGO/SPE motivated us to extend the immobilization technique towards the

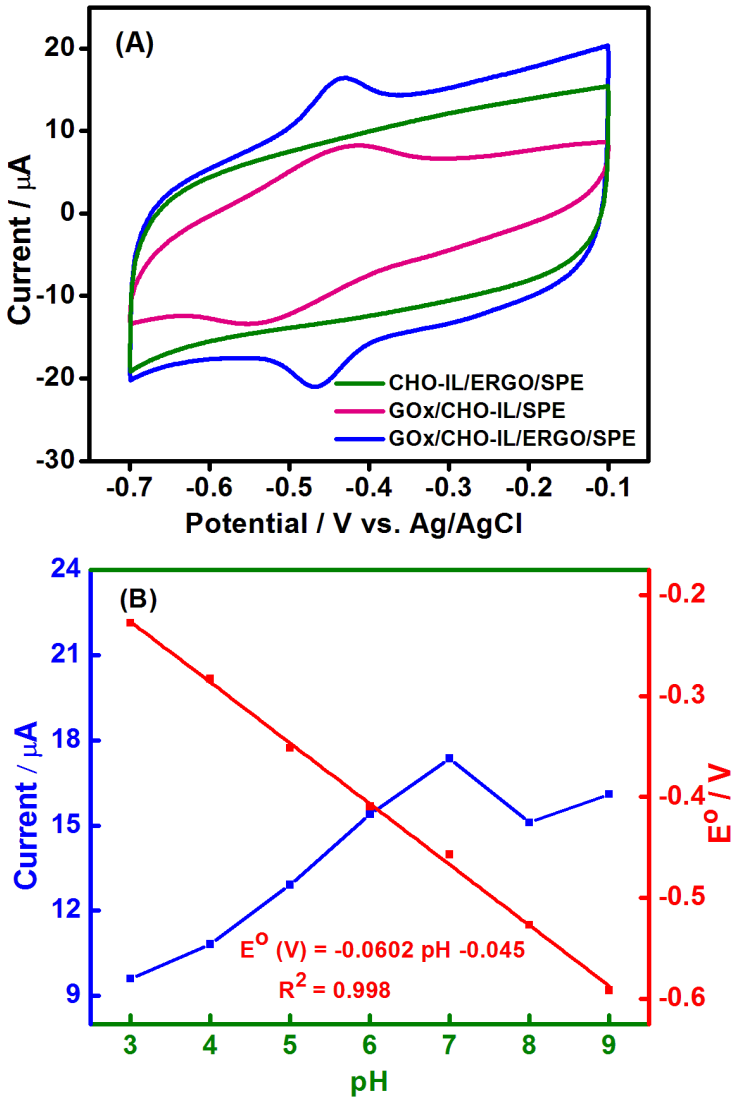

Figure 5. (A) CVs of CHO-IL/ERGO/SPE, GOx/CHO-IL/SPE and GOx/CHO-IL/ERGO/SPE (B) Effect of pH on the peak current and formal potential of the GOx/CHO-IL/ERGO/SPE. Electrolyte: 0.1 M N_2 saturated phosphate buffer (pH 7.0); Scan rate: 100 mV s^{-1}.

development of a mediatorless biosensor and accordingly GOx was immobilized onto CHO-IL for the fabrication of GOx/CHO-IL/ERGO/SPE. CVs recorded in N_2 saturated 0.1 M phosphate buffer (pH 7.0) at a scan rate of 100 mV s^{-1} during different stages of GOx immobilization are

presented in Figure 5A. The illustration shows no redox peaks for CHO-IL/ERGO/SPE, whereas GOx/CHO-IL/SPE exhibited a pair of peaks with the E_{pa} and E_{pc} of -0.428 and -0.546 V, corresponding to the redox behaviour of GOx, characteristic of the electron transfer process of FAD/$FADH_2$ (flavin adenine dinucleotide) redox centre (eqn. 3). After introduction of ERGO, the CV of GOx/CHO-IL/ERGO/SPE exhibited well-resolved anodic and cathodic peaks with higher peak currents at E_{pa} and E_{pc} of -0.432 and -0.464 V. The formal potentials ($E°$) obtained with GOx/CHO-IL/SPE and GOx/CHO-IL/ERGO/SPE were calculated to be -0.487 and -0.448 V respectively, which are in accordance to the standard electrode potential exhibited by GOx (Mani et al., 2013; Kang et al., 2009; Lee et al., 2012). This redox behaviour suggests that the covalent attachment of GOx through CHO-IL accelerates the electron transfer between the electrode and the FAD active centre deeply embedded in the thick insulating protein shell, aiding direct electron transfer and maintaining the enzymatic redox behaviour of GOx. A higher peak current and lesser peak-to-peak separation of 32 mV was observed for GOx/CHO-IL/ERGO/SPE than that of GOx/CHO-IL/SPE (ΔE_p = 118 mV) and this clearly indicates that ERGO offers good electrical conductivity and high surface area to facilitate the high loading capacity of the enzyme. The surface coverage, Γ which is a direct measure of the surface oriented active species at the modified enzyme electrode was quantified by the formula, $\Gamma = Q/nFA$ where Q is the charge, n is the number of electrons transferred, F is the Faraday's constant and A is the electroactive surface area. Γ calculated from area under the peak in cyclic voltammetric scan for GOx/CHO-IL/ERGO/SPE was found to be 2.96 x 10^{-10} mol cm^{-2} which was comparable to or higher than the earlier reports (Cui et al., 2013; Shi et al., 2015; Thirumalraj et al., 2015) attained through the specific binding of the enzyme moieties through covalent immobilization.

$$GOx\ (FAD) + 2H^+ + 2e^- \longleftrightarrow GOx\ (FADH_2) \qquad (3)$$

FAD, the redox centre of GOx exhibits a two electron, two proton redox reaction in aqueous solution. Thus, pH has a significant influence on its redox behaviour and hence the effect of pH on the peak current and peak potential of GOx/CHO-IL/ERGO/SPE modified electrode has been investigated. It could be seen from Figure 5B that the cathodic peak current increased as the pH was raised from 3 to 7 beyond which the peak current decreased indicating the highest bioactivity of the electrode at pH 7 which is suitable for physiological conditions. Moreover, the formal potential ($E°$) exhibited a linear shift on varying the pH from 3 to 9. The linear plot of formal potential against the solution pH resulted with a slope of 60.2 mV/pH, which is close to the theoretical Nernstian value of 59.2 mV/pH and agreed well with the previous reports of FAD redox reaction (Wang et al., 2013; Xiang et al., 2015).

Electrochemical detection of glucose is extremely significant not only in the diagnosis and treatment of diabetes but also for the detection of various metabolic disorders, food-processing and biotechnological discipline (Turner 2013; Wang 2008; Nery et al., 2016; Jin et al., 2015). Indirect detection of glucose was done at GOx/CHO-IL/ERGO/SPE by following the O_2 consumption in aerated phosphate buffer in the presence of different concentrations of glucose. Figure 6A illustrates the voltammograms of the developed biosensor recorded in air saturated 0.1 M phosphate buffer (pH 7.0) at 100 mV s^{-1} in the range of -0.1 to -0.7 V. A huge cathodic current was observed for GOx/CHO-IL/ERGO/SPE in air-saturated phosphate buffer when compared to that at N_2 saturated phosphate buffer (Figure 5A), arising from the electrocatalytic reduction of O_2 at the modified electrode. When glucose was added to the air saturated buffer, the redox centre FAD is reduced to $FADH_2$ during glucose oxidation and reoxidised to FAD by O_2 consumption at the electrode/electrolyte interface.

$$GOx\ (FADH_2) + O_2 \longrightarrow GOx\ (FAD) + H_2O_2 \quad (4)$$

$$GOx\ (FAD) + glucose \longrightarrow GOx\ (FADH_2) + gluconolactone \quad (5)$$

Every addition of glucose resulted in increasing O_2 consumption and restriction of electrochemical reaction (eqn. 3) due to the enzymatic reactions (eqns. 4 and 5) and consequently decreased the cathodic current. The decrease in cathodic current was proportional to the concentration of glucose added, which forms the basis for the development of glucose biosensor. The immobilization strategy and the nature of host matrix are the predominant factors in maintaining the native activity of the enzyme for electrocatalytic applications and both these factors are advantageously coupled to benefit the biosensor performance in this work.

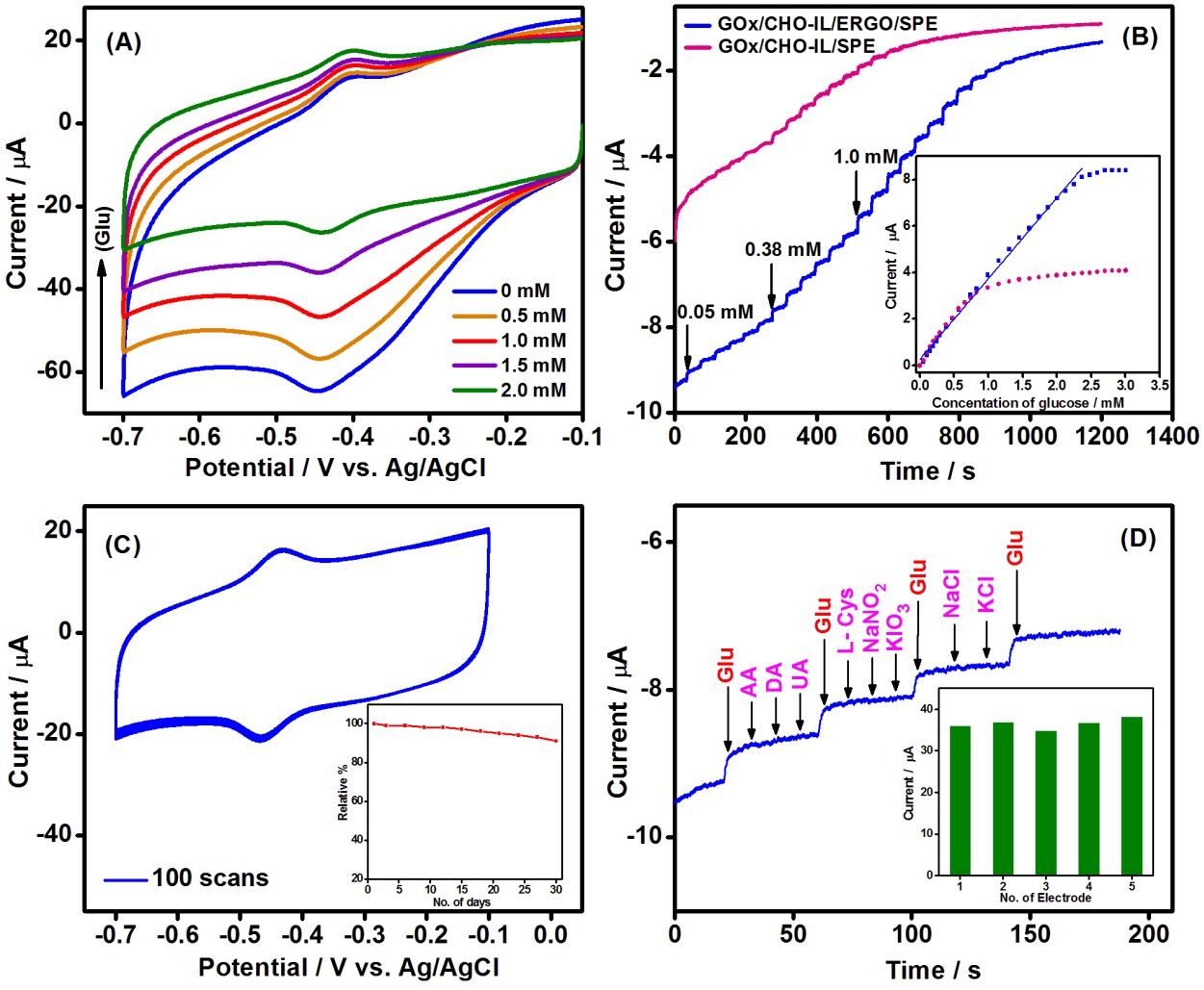

Figure 6. (A) CV curves of GOx/CHO-IL/ERGO/SPE with different concentration of glucose. (B) Amperometric response of GOx/CHO-IL/SPE and GOx/CHO-IL/ERGO/SPE on successive additions of different concentrations of glucose into stirred electrolyte; Applied potential: -0.45 V. Inset: Calibration plots corresponding to the amperometric response. (C) CVs of GOx/CHO-IL/ERGO/ SPE in 0.1 M N_2 saturated phosphate buffer (pH 7.0) for 100 continuous cycles at a scan rate of 100 mV s^{-1}. Inset: Long term stability of GOx/CHO-IL/ERGO/SPE over 30 days storage period. (D) Amperometric response of GOx/CHO-IL/ERGO/SPE towards the addition of 0.15 mM glucose and 1 mM of various interfering species such as ascorbic acid, dopamine, uric acid, L-cysteine, $NaNO_2$, KIO_3, NaCl and KCl in a stirred electrolyte. Inset: Current response columnar diagram for the response of glucose for five identically prepared GOx/CHO-IL/ERGO/SPE electrodes. Electrolyte: 0.1 M air saturated phosphate buffer (pH 7.0); Scan rate: 100 mV s^{-1}.

Quantification of glucose was carried out using amperometry at an applied potential of -0.45 V, since the CVs of GOx modified electrodes (Figure 6A) exhibited maximum cathodic peak current at this potential. Figure 6B shows the typical current-time curve at GOx/CHO-IL/SPE and GOx/CHO-IL/ERGO/SPE upon successive additions of glucose in an air saturated solution of 0.1 M phosphate buffer (pH 7.0). The current obtained at the FAD redox potential gradually decreases for each addition of glucose at both the modified electrodes. A non-linear and relatively poor response was observed with GOx/CHO-IL/SPE. Noticeably, the GOx/CHO-IL/ERGO/SPE has shown a sharp response for every addition of glucose and linearity was observed between glucose concentration and catalytic current in the wide range of 0.05 to 2.4 mM with a sensitivity and detection limit of 17.7 μA mM^{-1} cm^{-2} and 17 μM, respectively. The

results are comparable with or better than the recently reported mediatorless GOx based biosensors (Table S3). The electrocatalytic oxidation of glucose at GOx/CHO-IL/ERGO/SPE was very fast as the steady-state current was attained within 3 s. A notable sensing behaviour from the buried active sites of the GOx enzyme was brought about by the abundant conductivity of covalently linked IL and the ERGO in the biosensor setup. The developed biosensor acts as a promising sensing platform for glucose revealed from the analytical parameters achieved in the absence of any mediator.

The GOx/CHO-IL/ERGO/SPE was subjected to continuous potential cycling and Figure 6C shows no significant change in peak potentials or peak current could be observed even after 100 cycles. Also, the biosensor was assayed over 30 days at regular intervals of 3 days, towards the sensing of 1.5 mM glucose. As shown in the inset to Figure 6C, the biosensor retained its activity without any appreciable change during the initial 12 days of analysis and 91 % performance at the end of 30 days, displaying an acceptable long-term stability. When not in use, the GOx biosensor was stored dry at 4 °C. The reproducibility of electrode fabrication was established by the construction of five different freshly prepared GOx/CHO-IL/ERGO/SPE and the direct electrochemistry of GOx was examined with 1.5 mM glucose. A relative standard deviation of 3.3 % was observed among the individual electrodes (inset to Figure 6D), showing the good electrode reproducibility. The high stability of the biosensor is achieved through the strong covalent binding of GOx through a simple immobilization strategy. The biocompatible micro environment provided by IL and ERGO is also favourable for the orientation of the enzyme to retain the native activity and for the improved stability of the biosensor.

The selectivity of the biosensor is always desirable in real-time analysis as sample pre-treatment is not possible. The selectivity of glucose sensing was tested by examining glucose in

the presence of other possible electroactive species in biological medium by amperometry at an operating potential of -0.45 V (Figure 6D). The amperometric current of the biosensor decreased only towards the addition of 0.15 mM glucose and was not influenced even upon the addition of 1 mM ascorbic acid, dopamine, uric acid, L-cysteine, $NaNO_2$, KIO_3 and chloride ion. The interference free detection of glucose is attributed to the mediator-less direct electrochemistry of GOx and is advantageous for limiting the interference from biological mixtures.

The applicability of the developed biosensor is crucial and was evaluated by the determination of glucose in human serum samples. A standard addition method was followed by spiking known concentrations of glucose into the serum samples and examined their recovery using amperometry (Figure S17). The recoveries ranging from 97.8 to 101.6% were obtained (Table S4) for the estimation of glucose using the GOx biosensor. The results proved the suitability of the developed system towards sensing glucose in the physiological medium owing to the sensitivity and the selectivity derived from the cogent design of the biosensor.

4. Conclusion

To summarize, we report an aldehyde functionalized IL on ERGO as a new kind of versatile sensing platform, suitable for the immobilization of both chemical species such as Azu-A as well as a biocatalyst like GOx, which has the ability to overcome the shortcomings of existing sensors for electrocatalysis and bioelectrocatalytic process. The remarkable electrochemical and electrocatalytic behaviour of the designed sensors are a result of many cooperative contributions such as the effective immobilization of CHO-IL via π-π stacking of hydroxybenzyl and imidazolium groups on ERGO and direct covalent linkage of the mediator/enzyme in the electrode setup. The aldehyde functionalized IL on ERGO served as versatile host matrix maintaining apt microenvironment for the covalent immobilization of

enzyme/mediator as well as the improved charge transfer conductivity. The high surface area of ERGO ensured an increased loading of the mediator/enzyme apart from providing an excellent electron tunneling path for improved conductivity and sensitivity. The analytical characteristics obtained with both the H_2O_2 sensor and glucose biosensor are promising for real time appliance in terms of broad linear range, competent sensitivity, lower detection limit and interference-free detection. Structural fine tuning of ILs and their rational utilization in sensor design opens avenue for the development of sensors for desired plethora of applications.

Supporting Information

Supplementary data associated with this article can be found in the online version.

Acknowledgment

Science and Engineering Research Board (SERB), Government of India (Sanction No. SB/FT/CS-018/2014) is gratefully acknowledged for the financial support. The authors are also thankful for the financial help provided by RGEMS, VIT University, Vellore.

References

Armand, M., Endres, F., MacFarlane, D.R., Ohno, H., Scrosati, B., 2009. Nat. Mater. 8, 621–629.

Bai, Y.F., Xu, T.B., Luong, J.H.T., Cui, H.F., 2014. Anal. Chem. 86, 4910–4918.

Ballesta-Claver, J., Ametis-Cabello, J., Morales-Sanfrutos, J., Megía-Fernández, A., Valencia-Mirón, M.C., Santoyo-González, F., Capitán-Vallvey, L.F., 2012. Anal. Chim. Acta 754, 91–98.

Benjamin, M., Manoj, D., Thenmozhi, K., Bhagat, P.R., Saravanakumar, D., Senthilkumar, S., 2017. Biosens. Bioelectron. 91, 380–387.

Cao, S., Fang, L., Zhao, Z., Ge, Y., Piletsky, S., Turner, A.P.F., 2013. Adv. Funct. Mater. 23, 2162–2167.

Chen, Y-H., Kirankumar R., Huang, A.Y-T., Lu, C-Y., Kao, C-L., Chen, P-Y., 2015. Electrochim. Acta 184, 316-322.

Cui, M., Xu, B., Hu, C., Shao, H.B., Qu, L., 2013. Electrochim. Acta 98, 48–53.

Erramuspe, I.B.V., Fazeli, E., Nareoja, T., Trygg, J., Hanninen, P., Heinze, T., Fardim, P., 2016. Biomacromolecules 17, 3188–3197.

Etienne, M., Zhang, L., Vilà, N., Walcarius, A., 2015. Electroanalysis 27, 2028–2054

Ghica, M.E., Pauliukaite, R., Fatibello-Filho, O., Brett, C.M.A., 2009. Sens. Actuators B 142, 308–315.

Giernoth, R., 2010. Angew. Chemie Int. Ed. 49, 2834–2839.

Guohua, H., Hongyang, L., Zhiming, J., Danhua, Z., Haifang, W., 2017. Biosens. Bioelectron. 97, 184–195.

Haghighi, B., Khosravi, M., Barati, A., 2014. Mater. Sci. Eng. C 40, 204-211.

Hagiwara, R., Ito, Y., 2000. J. Fluor. Chem. 105, 221–227.

Han, Z., Li, F., Shu, J., Gao, L., Liu, X., Cui, H., 2016. ACS Appl. Mater. Interfaces 8, 17454–17460.

Hapiot, P., Lagrost, C., 2008. Chem. Rev. 108, 2238–2264.

Huang, J., Zheng, J., Sheng, Q., 2011. Microchim. Acta 173, 157-163.

Huddleston, J.G., Visser, A.E., Reichert, W.M., Willauer, H.D., Broker, G.A., Rogers, R.D., 2001. Green Chem. 3, 156–164.

Hui, G., Zhang, J., Li, J., Zheng, L., 2016. Food Chem. 197, 1168–1176.

Hummers, W.S., Offeman, R.E., 1958. J. Am. Chem. Soc. 80, 1339–1339.

Jiaojiao, J., Yangyang, G., Gangying, Z., Yanping, C., Wei, L., Guohua, H., 2015. Food Chem. 175, 485-493.

Jin, J., Zheng, G., Ge, Y., Deng, S., Liu, W., Hui, G., 2015. Electrochim. Acta 153, 594-601.

Kang, X., Wang, J., Wu, H., Aksay, I.A., Liu, J., Lin, Y., 2009. Biosens. Bioelectron. 25, 901–905.

Kim, J., Park, S.-J., Min, D.-H., 2017. Anal. Chem. 89, 232–248.

Kumar-Krishnan, S., Hernandez-Rangel, A., Pal, U., Ceballos-Sanchez, O., Flores-Ruiz, F.J., Prokhorov, E., Arias de Fuentes, O., Esparza, R., Meyyappan, M., 2016. J. Mater. Chem. B 4, 2553–2560.

Kwak, K., SenthilKumar, S., Pyo, K., Lee, D., 2014. ACS Nano 8, 671–679.

Lee, S., Ringstrand, B.S., Stone, D.A., Firestone, M.A., 2012. ACS Appl. Mater. Interfaces 4, 2311–2317.

Liu, J., He, Z., Khoo, S.Y., Tan, T.T.Y., 2016. Biosens. Bioelectron. 77, 942–949.

Mahmoud, K.A., Male, K.B., Hrapovic, S., Luong, J.H.T., 2009. ACS Appl. Mater. Interfaces 1, 1383–1386.

Mandegani, Z., Asadi, Z., Asadi, M., Karbalaei-Heidari, H.R., Rastegari, B., 2016. Dalton Trans. 45, 6592–6611.

Mani, V., Devadas, B., Chen, S.M., 2013. Biosens. Bioelectron. 41, 309–315.

Maroneze, C.M., dos Santos, G.P., de Moraes, V.B., da Costa, L.P., Kubota, L.T., 2016. Biosens. Bioelectron. 77, 746–751.

Mondal, K., Ali, M.A., Singh, C., Sumana, G., Malhotra, B.D., Sharma, A., 2017. Sens. Actuators B 246, 202–214.

Nery, E.W., Kundys, M., Jeleń, P.S., Jönsson-Niedziółka, M., 2016. Anal. Chem. 88, 11271–11282.

Pauliukaite, R., Ghica, M.E., Fatibello-Filho, O., Brett, C.M.A., 2010. Electrochim. Acta 55, 6239–6247.

Pereiro, A.B., Araujo, J.M.M., Martinho, S., Alves, F., Nunes, S., Matias, A., Duarte, C.M.M., Rebelo, L.P.N., Marrucho, I.M., 2013. ACS Sustain. Chem. Eng. 1, 427–439.

Priya, C., Sivasankari, G., Narayanan, S.S., 2012. Colloids Surf., B 97, 90-96.

Quinn, B.M., Ding, Z., Moulton, R., Bard, A.J., 2002. Langmuir 18, 1734–1742.

Safavi, A., Maleki, N., Farjamia, E., 2009. Electroanalysis 21, 1533-1538.

Sassolas, A., Blum, L.J., Leca-bouvier, B.D., 2012. Biotechnol. Adv. 30, 489–511.

Shi, Y., Li, X., Ye, M., Hu, C., Shao, H., Qu, L., 2015. J. Electrochem. Soc. 162, B138–B144.

Snehalatha, M., Joe, I.H., Ravikumar, C., Jayakumar, V.S., 2009. J. Raman Spectrosc. 40, 176–182.

Sprenger, K.G., Plaks, J.G., Kaar, J.L., Pfaendtner, J., 2017. Phys. Chem. Chem. Phys. 19, 17426–17433.

Sun, W., Gong, S., Shi, F., Cao, L., Ling, L., Zheng, W., Wang, W., 2014. Mater. Sci. Eng. C 40, 235-241.

Thenmozhi, K., Narayanan, S.S., 2017. Mater. Sci. Eng. C 70, 223–230.

Thirumalraj, B., Palanisamy, S., Chen, S.M., Yang, C.-Y., Periakaruppan, P., Lou, B.-S., 2015. RSC Adv. 5, 77651–77657.

Torimoto, T., Tsuda, T., Okazaki, K.I., Kuwabata, S., 2010. Adv. Mater. 22, 1196–1221.

Turner, A.P.F., 2013. Chem. Soc. Rev. 42, 3184-3196.

Unnikrishnan, B., Palanisamy, S., Chen, S., 2013. Biosens. Bioelectron. 39, 70–75.

Walcarius, A., Minteer, S.D., Wang, J., Lin, Y., Merkoci, A., 2013. J. Mater. Chem. B 1, 4878–4908.

Wang, H., Lang, Q., Li, L., Liang, B., Tang, X., Kong, L., Mascini, M., Liu, A., 2013. Anal. Chem. 85, 6107–6112.

Wang, J., 2008. Chem. Rev. 108 (2), 814-825.

Wasilewski, T., Gebicki, J., Kamysz, W., 2017. TrAC - Trends Anal. Chem. 93, 23–36.

Xiang, D., Yin, L., Ma, J., Guo, E., Li, Q., Li, Z., Liu, K., 2015. Analyst 140, 644–653.

Yang, Y., Yan, Q., Liu, Q., Li, Y., Liu, H., Wang, P., Chen, L., Zhang, D., 2018. Biosens. Bioelectron. 99, 450–457.

Yu, S., Wang, X., Yao, W., Wang, J., Ji, Y., Ai, Y., Alsaedi, A., Hayat, T., Wang, X., 2017. Environ. Sci. Technol. 51, 3278–3286.

Zhang, L., Zhang, Q., Li, J., 2010. Biosens. Bioelectron. 26, 846–849.

Zhang, W., Xu, Y., Zou, X., Wang, P., 2017. Biosens. Bioelectron. 97, 267–272.

Zhao, M., Gao, Y., Sun, J., Gao, F., 2015. Anal. Chem. 87, 2615–2622.

Graphical Abstract

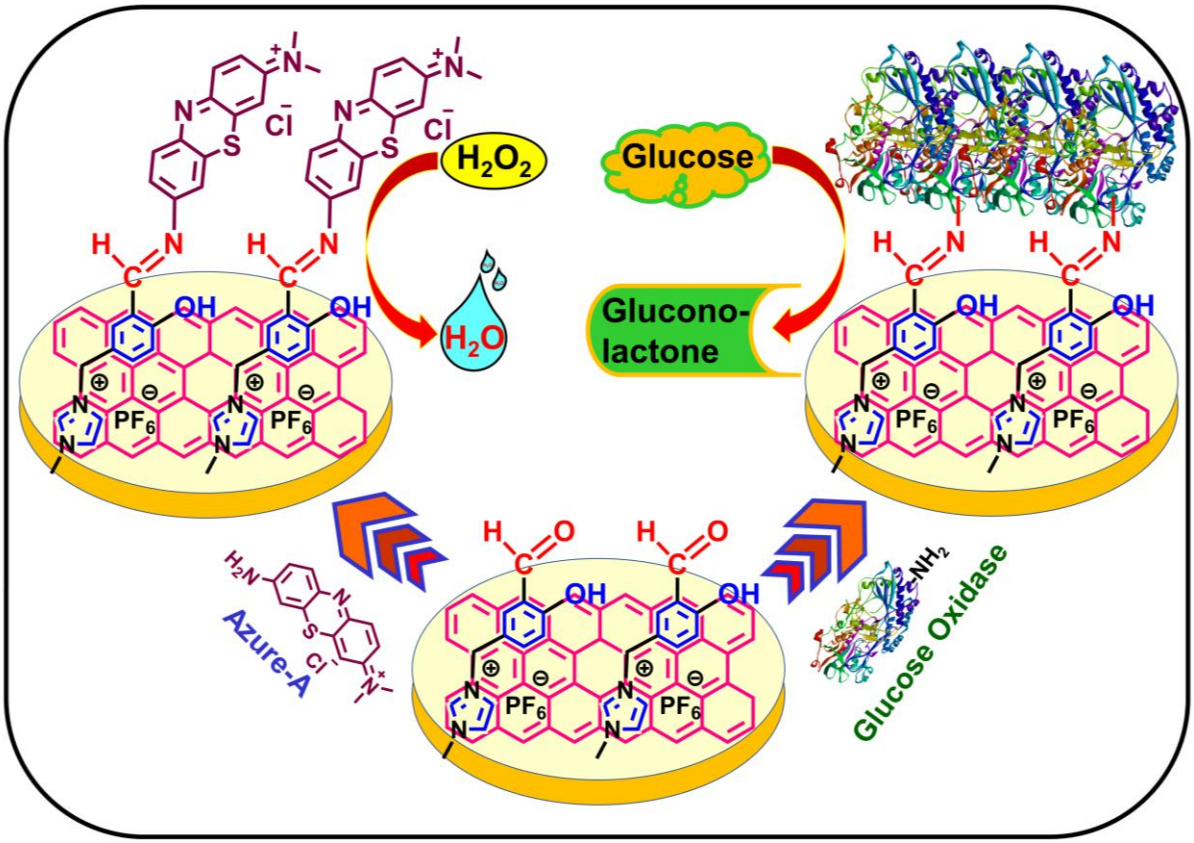

Highlights

- Aldehyde functionalized ionic liquid was synthesized and characterized
- CHO-IL on ERGO demonstrated as a platform for covalent immobilization of biomolecules
- Azure A immobilized on the new platform, utilized for nonenzymatic sensing of H_2O_2
- Glucose biosensor developed through immobilization of glucose oxidase on CHO-IL